Journal of Applied Physics

Acoustic radiation force and motion of a free cylinder in a viscous fluid with a boundary defined by a plane wave incident at an arbitrary angle

Cite as: J. Appl. Phys. **128**, 044902 (2020); https://doi.org/10.1063/5.0005866
Submitted: 26 February 2020 . Accepted: 08 July 2020 . Published Online: 24 July 2020

Yupei Qiao, Xiaowei Zhang, Menyang Gong, Haibin Wang, and Xiaozhou Liu

AIP Publishing

Journal of Applied Physics ARTICLE scitation.org/journal/jap

Acoustic radiation force and motion of a free cylinder in a viscous fluid with a boundary defined by a plane wave incident at an arbitrary angle

Cite as: J. Appl. Phys. **128**, 044902 (2020); doi: 10.1063/5.0005866
Submitted: 26 February 2020 · Accepted: 8 July 2020 ·
Published Online: 24 July 2020

Yupei Qiao,[1] Xiaowei Zhang,[1] Menyang Gong,[1] Haibin Wang,[1] and Xiaozhou Liu[1,2,a)]

AFFILIATIONS

[1]Key Laboratory of Modern Acoustics, Institute of Acoustics and School of Physics, Nanjing University, Nanjing 210093, China
[2]State Key Laboratory of Acoustics, Institute of Acoustics, Chinese Academy of Sciences, Beijing 100190, China

[a)]**Author to whom correspondence should be addressed:** xzliu@nju.edu.cn

ABSTRACT

The acoustic radiation force (ARF) is derived for a free cylinder immersed in a viscous fluid with a boundary defined by a plane wave incident at an arbitrary angle. Trajectories of a free rigid cylinder under the action of ARF are also investigated. Various aspects affecting the ARFs and trajectories of a free rigid cylinder, such as fluid viscosity, the incident angle of the plane wave, the density ratio of the fluid to particle, the particle radius, and boundary, are addressed in numerical simulations. Results show that ARFs are positive or negative depending on the various factors considered in this work. Moreover, the amplitude of the total ARF on a free cylinder in a bounded viscous fluid defined by a plane wave incident at a certain angle may decrease with increasing viscosity, which is significantly different from the case of a fixed cylinder immersed in a boundless viscous fluid. Furthermore, the trajectory of the particle changing with different conditions is investigated. We can predict and regulate the particle trajectory by selecting relevant parameters. The finite element method is implemented to validate the theoretical results. The finite element results and theoretical results are in good agreement. This work helps better understand the underlying mechanism of the particle manipulation using ARF.

I. INTRODUCTION

Manipulation of particles using acoustic radiation force (ARF) becomes the subject of numerous studies for its applications in various areas, such as material science, ultrasonic medicine, biophysics, industry, etc.[1–11] The study of ARF has a long history[12] beginning with works by King[13] and Yosioka and Kawasima.[14] Most of the works have focused on the case of an ideal fluid, where the viscosity is neglected, or fixed particle.[15–32] However, viscosity always exists in practical applications of ARF. Moreover, the particle generally starts moving under the action of ARF. The problem of ARFs on particles immersed in a viscous fluid within an axisymmetric sound field has been discussed and analyzed.[33–42]

Nevertheless, the assumption of axisymmetry is not appropriate in many situations. The present work deals with the ARF on a free cylinder in a real fluid (i.e., a viscous fluid with a boundary defined by a plane wave incident at an arbitrary angle). Expressions of axial and transverse ARFs are derived. The solutions obtained here are the case of an arbitrary incident plane wave sound field not necessarily axisymmetric. Additionally, we consider the effect of viscosity in a bounded sound field not necessarily a low viscosity or ideal fluid or unbounded region. The theoretical study of this problem is challenging. To put it more exactly, we consider various factors affecting ARFs, such as fluid viscosity, incident angle of the plane wave, density ratio of the fluid to particle, particle radius, and position. Moreover, physical explanations for various aspects affecting ARFs are discussed in detail. Furthermore, the trajectories of particles with various radii under the action of ARF are calculated. Note that the analytical solution of the ARF presented in this paper can be applied to calculate the ARF on any free cylinder in a viscous fluid with a boundary defined by a plane wave incident at an arbitrary angle. We assume that the cylinder is rigid in numerical simulations to simply and clearly explain the effect of viscosity and the motion of particles in the arbitrary bounded plane wave field. Finally, the comparisons between the results obtained adopting the finite element method (FEM) and those calculated by the theory are performed.

II. THEORY

A. Scattering of sound waves by a free cylinder immersed in a viscous fluid with a rigid boundary defined by a plane wave incident at an arbitrary angle

Considering a free cylinder, which is assumed to be rigid, infinitely long, isotropic, and homogeneous, with radius R immersed in a viscous fluid at a distance d from a rigid boundary. All disturbances generated by the incident wave are assumed to be so small that the linearized theory of viscous liquid is applicable. A main Cartesian coordinate system (x, y) is set as shown in Fig. 1. A plane wave is incident at an angle θ $(-\pi/2 \le \theta \le \pi/2)$. The flat boundary reflects this wave unless $|\theta| = \pi/2$. The method of images is applied to describe reflection from the boundary. Accordingly, an image cylinder having the same size as the original cylinder and an image plane wave mirrored at the boundary are introduced (Fig. 1). Two cylindrical coordinate systems (r_1, φ_1) and (r_2, φ_2) centered, respectively, on the original cylinder and image cylinder are established.

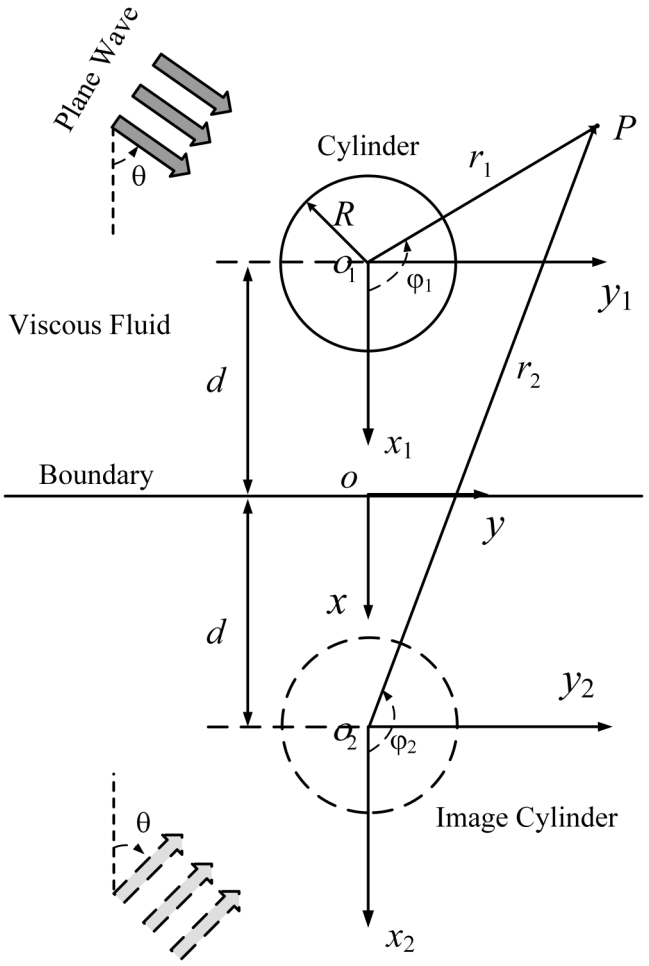

FIG. 1. Geometrical configuration of a free rigid cylinder immersed in a viscous fluid with a boundary defined by a plane wave incident at an arbitrary angle.

The velocity potential for a plane wave incident at an angle θ is represented in systems (r_1, φ_1) as

$$\Phi_{\text{int}} = A \sum_{n=-\infty}^{\infty} i^n J_n(\alpha r_1) e^{in(\varphi_1 - \theta)} e^{-i\alpha d \cos\theta} e^{-i\omega t}, \tag{1}$$

where $A = \sqrt{2I_0/\rho_0 c_0 k^2}$ is the amplitude, I_0 is the intensity of the incident wave, ρ_0 and c_0 are the density and speed of sound in a viscous liquid, respectively, $\alpha = (\omega/c_0)[1 - i\omega(\lambda' + 2\mu')/\rho_0 c_0^2]^{-1/2}$ is the complex wave number of a longitudinal wave, $k = \text{Re}(\alpha)$, ω is the angular frequency, t is the time, and $J_n(\cdot)$ is the nth-order Bessel function of the first kind. Parameters λ' and μ' denote the second viscosity coefficient and dynamic viscosity coefficient, respectively.

The scattering problem of the incident wave by a free cylinder may be reduced to finding potentials Φ_l and Ψ_t as solutions of the acoustic equation,[43,44]

$$\left[\left(1 + \frac{\lambda' + 2\mu'}{c_0^2 \rho_0}\frac{\partial}{\partial t}\right)\Delta - \frac{1}{c_0^2}\frac{\partial^2}{\partial t^2}\right]\Phi_l = 0, \tag{2}$$

$$\left(\nu\Delta - \frac{\partial}{\partial t}\right)\Psi_t = 0, \quad \nu = \frac{\mu'}{\rho_0}, \tag{3}$$

where ν is the kinematic viscosity coefficient. The solutions of Eqs. (2) and (3) can be written as

$$\Phi_l^{(1)} = \sum_{n=-\infty}^{\infty} A_n^{(1)} H_n^{(1)}(\alpha r_1) e^{in\varphi_1} e^{-i\omega t}, \tag{4}$$

$$\Psi_t^{(1)} = \sum_{n=-\infty}^{\infty} B_n^{(1)} H_n^{(1)}(\beta r_1) e^{in\varphi_1} e^{-i\omega t}, \tag{5}$$

where $\Phi_l^{(1)}$ and $\Psi_t^{(1)}$ are the potentials of scattered longitudinal and transverse waves by the free cylinder, respectively, $A_n^{(1)}$ and $B_n^{(1)}$ are scattering coefficients determined by boundary conditions at the lateral surface of the cylinder, $H_n^{(1)}(\cdot) = J_n(\cdot) + iY_n(\cdot)$ is the nth-order Hankel function of the first kind, $\beta = (1 + i)/\delta$ is the wave number of the shear wave, and $\delta = (2\mu'/\rho_0\omega)^{1/2}$ is the depth of penetration of the viscous wave.

Using the method of images, we obtain the potentials of the reflected wave (Φ_r) from the boundary, scattered longitudinal $\Phi_l^{(2)}$, and transverse $\Psi_t^{(2)}$ waves by the image cylinder in their respective coordinate systems,

$$\Phi_r = A \sum_{n=-\infty}^{\infty} i^n J_n(\alpha r_1) e^{-in(\pi - \varphi_1 - \theta)} e^{i\alpha d \cos\theta} e^{-i\omega t}, \tag{6}$$

$$\Phi_l^{(2)} = \sum_{n=-\infty}^{\infty} A_n^{(2)} H_n^{(1)}(\alpha r_2) e^{in\varphi_2} e^{-i\omega t}, \tag{7}$$

$$\Psi_t^{(2)} = \sum_{n=-\infty}^{\infty} B_n^{(2)} H_n^{(1)}(\beta r_2) e^{in\varphi_2} e^{-i\omega t}, \tag{8}$$

where $A_n^{(2)} = (-1)^n A_n^{(1)}$ and $B_n^{(2)} = (-1)^n B_n^{(1)}$.

To calculate scattering coefficients, we transform Eqs. (7) and (8) into the coordinate system (r_1, φ_1) by applying the addition theorem for the cylindrical wave function,[45]

$$\Phi_l^{(2)\prime} = \sum_{n=-\infty}^{\infty}\sum_{m=-\infty}^{\infty}(-1)^m A_m^{(1)} H_{n-m}^{(1)}(2\alpha d) J_n(\alpha r_1) e^{in\varphi_1} e^{-i\omega t}, \quad (9)$$

$$\Psi_t^{(2)\prime} = \sum_{n=-\infty}^{\infty}\sum_{m=-\infty}^{\infty}(-1)^m B_m^{(1)} H_{n-m}^{(1)}(2\beta d) J_n(\beta r_1) e^{in\varphi_1} e^{-i\omega t}. \quad (10)$$

From Eqs. (1), (4)–(6), (9), and (10), the total potential of the velocity field is obtained as

$$\begin{aligned}\Phi &= \Phi_i + \Phi_r + \Phi_l^{(1)} + \Phi_l^{(2)\prime} \\ &= \sum_{n=-\infty}^{\infty}\left[2A\cos\left(\alpha d\cos\theta + n\theta - \frac{n\pi}{2}\right) J_n(\alpha r_1) + A_n^{(1)} H_n^{(1)}(\alpha r_l) + S_n J_n(\alpha r_1)\right] e^{in\varphi_1} e^{-i\omega t},\end{aligned} \quad (11)$$

$$\begin{aligned}\Psi &= \Psi_l^{(1)} + \Psi_l^{(2)\prime} \\ &= \sum_{n=-\infty}^{\infty}[B_n^{(1)} H_n^{(1)}(\beta r_l) + Q_n J_n(\beta r_1)] e^{in\varphi_1} e^{-i\omega t},\end{aligned} \quad (12)$$

where

$$S_n = \sum_{m=-\infty}^{\infty}(-1)^m A_m^{(1)} H_{n-m}^{(1)}(2\alpha d),$$

$$Q_n = \sum_{m=-\infty}^{\infty}(-1)^m B_m^{(1)} H_{n-m}^{(1)}(2\beta d).$$

In the later calculation of the ARF, we express Eqs. (11) and (12) as

$$\Phi = \sum_{n=-\infty}^{\infty}(G_n + iL_n) e^{in\varphi_1} e^{-i\omega t}, \quad (13)$$

$$\Psi = \sum_{n=-\infty}^{\infty}(M_n + iN_n) e^{in\varphi_1} e^{-i\omega t}, \quad (14)$$

where

$$G_n = \mathrm{Re}\left[2A\cos\left(\alpha d\cos\theta + n\theta - \frac{n\pi}{2}\right) J_n(\alpha r_1) + A_n^{(1)} H_n^{(1)}(\alpha r_l) + S_n J_n(\alpha r_1)\right],$$

$$L_n = \mathrm{Im}\left[2A\cos\left(\alpha d\cos\theta + n\theta - \frac{n\pi}{2}\right) J_n(\alpha r_1) + A_n^{(1)} H_n^{(1)}(\alpha r_l) + S_n J_n(\alpha r_1)\right],$$

$$M_n = \mathrm{Re}[B_n^{(1)} H_n^{(1)}(\beta r_l) + Q_n J_n(\beta r_1)],$$

$$N_n = \mathrm{Im}[B_n^{(1)} H_n^{(1)}(\beta r_l) + Q_n J_n(\beta r_1)].$$

For an ideal fluid ($\lambda' = 0,\ \nu = 0$ and $\mu' = 0$),

$$\begin{aligned}G_n &= \left[2A\cos\left(kd\cos\theta + n\theta - \frac{n\pi}{2}\right) + A_n^{(1)\prime} + S'_n\right] J_n(kr_1) - A_n^{(1)\prime\prime} Y_n(kr_1), \\ L_n &= A_n^{(1)\prime} Y_n(kr_1) + (A_n^{(1)\prime\prime} + S''_n) J_n(kr_1),\end{aligned}$$

in which $A_n^{(1)\prime} = \mathrm{Re}(A_n^{(1)})$, $S'_n = \mathrm{Re}(S_n)$, $A_n^{(1)\prime\prime} = \mathrm{Im}(A_n^{(1)})$, and $S'' = \mathrm{Im}(S_n)$ while $\mathrm{Re}(\cdot)$ and $\mathrm{Im}(\cdot)$ denote real and imaginary parts, respectively.

The boundary condition at the lateral surface of cylinder is

$$\mathbf{v} = \mathbf{U}, \quad (15)$$

where $\mathbf{U}$ is the velocity vector of the object. The acoustic field is affected by the motion of the particle, so it is introduced as a boundary condition. $\mathbf{U}$ is obtained from the dynamical equation,

$$m\dot{\mathbf{U}} = \iint_{S_0} \boldsymbol{\sigma}\, dS, \quad (16)$$

where

$$\boldsymbol{\sigma} = (-p_1 + \lambda'\Delta \times \mathbf{v})\mathbf{E} + 2\mu'\mathbf{e}, \quad (17)$$

$$\begin{aligned}p_1 = \rho_0\left(\frac{\lambda' + 2\mu'}{\rho_0}\Delta - \frac{\partial}{\partial t}\right)\Phi + \frac{\rho_0}{2c_0}\left(\frac{\partial\Phi}{\partial t}\right)^2 - \frac{1}{2}\rho_0(\overrightarrow{\nabla\Phi})^2 \\ - \frac{\lambda' + 2\mu'}{c_0^2}\frac{\partial\Phi}{\partial t}\Delta\Phi,\end{aligned} \quad (18)$$

in which $\mathbf{E}$ is a unit tensor, $\mathbf{e} = ((\nabla\mathbf{v}) + (\nabla\mathbf{v})^{\mathrm{T}})/2$ is the deformation velocity tensor, the superscript T denotes vector transposition, $m = \pi R^2\rho_1$ is the mass of a unit length of the cylinder, ρ_1 is the density of the cylinder, and $\boldsymbol{\sigma}$ is the tensor of stresses. Since the dynamic equation is required merely at a later stage of calculating ARF, only the first-order contribution of the pressure field p_1 is taken into account and it is sufficiently accurate to determine the motion of the cylinder.[28]

The velocity vector $\mathbf{v}$ of the fluid is

$$\mathbf{v} = \nabla\Phi + \nabla \times \Psi. \quad (19)$$

Substituting Eqs. (11) and (12) into Eqs. (16)–(18) and applying the boundary conditions at the cylinder surface [Eq. (15)], we obtain the scattering coefficients in the following form:

$$(a - cf)X = b, \quad (20)$$

where

$$X = [A_{-n} \quad A_{-n+1} \quad \cdots \quad A_{-1} \quad A_0 \quad A_1 \quad \cdots \quad A_{n-1} \quad A_n ; B_{-n} \quad B_{-n+1} \quad \cdots \quad B_{-1} \quad B_0 \quad B_1 \quad \cdots \quad B_{n-1} \quad B_n]^T,$$

$$a = \begin{bmatrix} C_r & D_r \\ C_\varphi & D_\varphi \end{bmatrix},$$

$$b = [I_{r,-n} \quad I_{r,-n+1} \quad \cdots \quad I_{r,-1} \quad I_{r,0} \quad I_{r,1} \quad \cdots \quad I_{r,n-1} \quad I_{r,n} ; I_{\varphi,-n} \quad I_{\varphi,-n+1} \quad \cdots \quad I_{\varphi,-1} \quad I_{\varphi,0} \quad I_{\varphi,1} \quad \cdots \quad I_{\varphi,n-1} \quad I_{\varphi,n}]^T,$$

$$c = \begin{bmatrix} S_r & Q_r \\ S_\varphi & Q_\varphi \end{bmatrix},$$

$$f = \begin{bmatrix} W_{1n} & O \\ O & W_{2n} \end{bmatrix},$$

$$W_{1n} = \begin{bmatrix} (-1)^{-n}H_0^{(1)}(2\alpha d) & (-1)^{-n+1}H_{-1}^{(1)}(2\alpha d) & \cdots & (-1)^{n-1}H_{-2n+1}^{(1)}(2\alpha d) & (-1)^{n}H_{-2n}^{(1)}(2\alpha d) \\ (-1)^{-n}H_1^{(1)}(2\alpha d) & (-1)^{-n+1}H_0^{(1)}(2\alpha d) & \cdots & (-1)^{n-1}H_{-2n+2}^{(1)}(2\alpha d) & (-1)^{n}H_{-2n+1}^{(1)}(2\alpha d) \\ \vdots & \vdots & \ddots & \vdots & \vdots \\ (-1)^{-n}H_{2n-1}^{(1)}(2\alpha d) & (-1)^{-n+1}H_{2n-2}^{(1)}(2\alpha d) & \cdots & (-1)^{n-1}H_0^{(1)}(2\alpha d) & (-1)^{n}H_{-1}^{(1)}(2\alpha d) \\ (-1)^{-n}H_{2n}^{(1)}(2\alpha d) & (-1)^{-n+1}H_{2n-1}^{(1)}(2\alpha d) & \cdots & (-1)^{n-1}H_1^{(1)}(2\alpha d) & (-1)^{n}H_0^{(1)}(2\alpha d) \end{bmatrix},$$

$$W_{2n} = \begin{bmatrix} (-1)^{-n}H_0^{(1)}(2\beta d) & (-1)^{-n+1}H_{-1}^{(1)}(2\beta d) & \cdots & (-1)^{n-1}H_{-2n+1}^{(1)}(2\beta d) & (-1)^{n}H_{-2n}^{(1)}(2\beta d) \\ (-1)^{-n}H_1^{(1)}(2\beta d) & (-1)^{-n+1}H_0^{(1)}(2\beta d) & \cdots & (-1)^{n-1}H_{-2n+2}^{(1)}(2\beta d) & (-1)^{n}H_{-2n+1}^{(1)}(2\beta d) \\ \vdots & \vdots & \ddots & \vdots & \vdots \\ (-1)^{-n}H_{2n-1}^{(1)}(2\beta d) & (-1)^{-n+1}H_{2n-2}^{(1)}(2\beta d) & \cdots & (-1)^{n-1}H_0^{(1)}(2\beta d) & (-1)^{n}H_{-1}^{(1)}(2\beta d) \\ (-1)^{-n}H_{2n}^{(1)}(2\beta d) & (-1)^{-n+1}H_{2n-1}^{(1)}(2\beta d) & \cdots & (-1)^{n-1}H_1^{(1)}(2\beta d) & (-1)^{n}H_0^{(1)}(2\beta d) \end{bmatrix},$$

in which, submatrices C_r, C_φ, D_r, D_φ, S_r, S_φ, Q_r, and Q_φ are diagonal matrices with elements $C_{r,n}$, $C_{\varphi,n}$, $D_{r,n}$, $D_{\varphi,n}$, $S_{r,n}$, $S_{\varphi,n}$, $Q_{r,n}$, and $Q_{\varphi,n}$, respectively and O is a zero matrix with the same dimension as W_{1n} and W_{1n} matrices. The elements of these diagonal matrices and matrix b are expressed as

$$C_{r,n} = \gamma_{r,n},$$

$$\gamma_{r,n} = nH_n^{(1)}(\alpha r_1) - \alpha r_1 H_{n+1}^{(1)}(\alpha r_1),$$

$$D_{r,n} = i\delta_{r,n},$$

$$\delta_{r,n} = nH_n^{(1)}(\beta r_1),$$

$$I_{r,n} = -2A\cos\left(\alpha d\cos\theta + n\theta - \frac{n\pi}{2}\right)\beta_{r,n},$$

$$\beta_{r,n} = nJ_n(\alpha r_1) - \alpha r_1 J_{n+1}(\alpha r_1),$$

$$S_{r,n} = -\beta_{r,n},$$

$$Q_{r,n} = -i\chi_{r,n},$$

$$\chi_{r,n} = nJ_n(\beta r_1),$$

$$C_{\varphi,n} = i\gamma_{\varphi,n},$$

$$\gamma_{\varphi,n} = nH_n^{(1)}(\alpha r_1),$$

$$D_{\varphi,n} = -\delta_{\varphi,n},$$

$$\delta_{\varphi,n} = nH_n^{(1)}(\beta r_1) - \alpha r_1 H_{n+1}^{(1)}(\beta r_1),$$

$$I_{\varphi,n} = -2iA\cos\left(\alpha d\cos\theta + n\theta - \frac{n\pi}{2}\right)\beta_{\varphi,n},$$

$$\beta_{\varphi,n} = nJ_n(\alpha r_1),$$

$$S_{\varphi,n} = -i\beta_{\varphi,n},$$

$$Q_{\varphi,n} = \chi_{\varphi,n},$$

$$\chi_{\varphi,n} = nJ_n(\beta r_1) - \alpha r_1 J_{n+1}(\beta r_1) \qquad (|n| \neq 1),$$

$$C_{r,n} = \gamma_{r,n} - \eta\gamma_{\varphi,n},$$

$$D_{r,n} = i(1-\eta)\delta_{r,n},$$

$$I_{r,n} = 2A\sin(\alpha d\cos\theta + \theta)(\eta\beta_{\varphi,n} - \beta_{r,n}),$$

$$S_{r,n} = \eta\beta_{\varphi,n} - \beta_{r,n},$$

$$Q_{r,n} = i(\eta-1)\chi_{r,n},$$

$$C_{\varphi,n} = i\gamma_{\varphi,n} - i\eta\gamma_{r,n},$$

$$D_{\varphi,n} = -\delta_{\varphi,n} + \eta\delta_{r,n},$$

$$I_{\varphi,n} = 2iA\sin(\alpha d\cos\theta + \theta)(\eta-1)\beta_{\varphi,n},$$

$$S_{\varphi,n} = i(\eta-1)\beta_{\varphi,n},$$

$$Q_{\varphi,n} = -\eta\chi_{r,n} + \chi_{\varphi,n}$$

$$(n=1),$$

$$C_{r,n} = \gamma_{r,n} + \eta\gamma_{\varphi,n},$$

$$D_{r,n} = i(1-\eta)\delta_{r,n},$$

$$I_{r,n} = 2A\sin(\alpha d\cos\theta - \theta)(\eta\beta_{\varphi,n} + \beta_{r,n}),$$

$$S_{r,n} = -\eta\beta_{\varphi,n} - \beta_{r,n},$$

$$Q_{r,n} = i(\eta-1)\chi_{r,n},$$

$$C_{\varphi,n} = i\gamma_{\varphi,n} - i\eta\gamma_{r,n},$$

$$D_{\varphi,n} = -\delta_{\varphi,n} - \eta\delta_{r,n},$$

$$I_{\varphi,n} = 2iA\sin(\alpha d\cos\theta - \theta)(1-\eta)\beta_{\varphi,n},$$

$$S_{\varphi,n} = i(\eta-1)\beta_{\varphi,n},$$

$$Q_{\varphi,n} = \eta\chi_{r,n} + \chi_{\varphi,n}$$

$$(n=-1),$$

where $\eta = \rho_0/\rho_1$.

The scattering coefficients are computed by solving Eq. (20). Passing to the limit $\eta \to 0$ in Eq. (20), one obtains scattering coefficients for a fastened cylinder in a viscous fluid.

B. ARF on a free cylinder immersed in a viscous fluid with a boundary defined by a plane wave incident at an arbitrary angle

The time-averaged ARF acting on a cylinder immersed freely in a viscous fluid is[35]

$$\mathbf{F} = \left\langle \iint_{S_0} \boldsymbol{\sigma} dS \right\rangle, \tag{21}$$

where $\boldsymbol{\sigma}$ is expressed as Eq. (17) and $\langle\rangle$ represents the time average. Here, the stresses are calculated based on a simplified system of the nonlinear equations of hydromechanics. The nonlinear and dissipative terms are retained in the simplified system. All terms of p_1 [Eq. (18)] are considered and the partial derivative $\partial\Phi/\partial t$ for a free object is calculated by

$$\frac{\partial\Phi}{\partial t} = \frac{d\Phi}{dt} - \mathbf{U}\cdot\nabla, \tag{22}$$

since $\partial\Phi/\partial t$ should be calculated in a fixed coordinate system relative to which the velocity potential is determined. The last terms of Eq. (22) give rise to pressure contributions having the same order as that of the last three terms of Eq. (18).

The total ARF can be written as $\mathbf{F} = F_x\mathbf{e}_x + F_y\mathbf{e}_y$, where F_x and F_y are the axial and transverse forces, respectively, $\mathbf{e_x}$ and $\mathbf{e_y}$ are unit vectors in x and y axes, respectively.

Substituting Eqs. (13), (14), (17), (18), and (22) into Eq. (21), the axial and transverse ARFs are obtained as

$$\begin{aligned}
F_x = {} & \frac{\eta\rho_0\pi}{R}[-(G_1+N_1)G_2 - (L_1-M_1)L_2 + 2M_{-1}M_{-2} + (N_{-1}-G_{-1})G_{-2} - (L_{-1}+M_{-1})L_{-2} + L_{-1}M_{-2} - G_{-1}N_{-2}] \\
& - \frac{\pi R\rho_0\omega^2}{4c_0^2}\sum_{n=-\infty}^{\infty}(G_nG_{n+1} + L_nL_{n+1} + G_nG_{n-1} + L_nL_{n-1}) + \frac{\rho_0\pi}{4R}\sum_{n=-\infty}^{\infty} n(n+1)(N_nN_{n+1} + M_nM_{n+1}) + n(n-1)(N_nN_{n-1} + M_nM_{n-1}) \\
& + \frac{\rho_0\pi}{4R}\sum_{n=-\infty}^{\infty} n(n+1)(L_nL_{n+1} + G_nG_{n+1}) + n(n-1)(L_nL_{n-1} + G_nG_{n-1}) - \frac{\pi R\rho_0^2(\lambda'+2\mu')\omega^3}{2[\rho_0^2c_0^2 + \omega^2(\lambda'+2\mu')^2]} \\
& \sum_{n=-\infty}^{\infty}(L_nG_{n+1} + L_nG_{n-1} - G_nL_{n+1} - G_nL_{n-1}) + \frac{\pi R\rho_0(\lambda'+2\mu')^2\omega^4}{2c_0^2[\rho_0^2c_0^2 + \omega^2(\lambda'+2\mu')^2]}\sum_{n=-\infty}^{\infty}(G_nG_{n+1} + L_nL_{n+1} + G_nG_{n-1} + L_nL_{n-1}),
\end{aligned} \tag{23}$$

$$F_y = \frac{\eta\rho_0\pi}{R}[(G_1 - N_1)L_2 - (L_1 + M_1)G_2 + (L_{-1} + M_{-1})G_{-2} - (N_{-1} + G_{-1})L_{-2}]$$
$$-\frac{\pi R\rho_0\omega^2}{4c_0^2}\sum_{n=-\infty}^{\infty}(L_nG_{n+1} - G_nL_{n+1} - L_nG_{n-1} + G_nL_{n-1})$$
$$+\frac{\rho_0\pi}{4R}\sum_{n=-\infty}^{\infty}n(n+1)(-M_nN_{n+1} + N_nM_{n+1}) + n(n-1)(M_nN_{n-1} - N_nM_{n-1})$$
$$+\frac{\rho_0\pi}{4R}\sum_{n=-\infty}^{\infty}n(n+1)(L_nG_{n+1} - G_nL_{n+1}) + n(n-1)(G_nL_{n-1} - L_nG_{n-1})$$
$$-\frac{\pi R\rho_0^2(\lambda' + 2\mu')\omega^3}{2[\rho_0^2c_0^2 + \omega^2(\lambda' + 2\mu')^2]}\sum_{n=-\infty}^{\infty}(-L_nL_{n+1} + L_nL_{n-1} - G_nG_{n+1} + G_nG_{n-1})$$
$$+\frac{\pi R\rho_0(\lambda' + 2\mu')^2\omega^4}{2c_0^2[\rho_0^2c_0^2 + \omega^2(\lambda' + 2\mu')^2]}\sum_{n=-\infty}^{\infty}(L_nG_{n+1} - G_nL_{n+1} - L_nG_{n-1} + G_nL_{n-1}). \quad (24)$$

Passing to the limit $\lambda', \mu' \to 0$ in Eqs. (23) and (24), we have ARFs on a cylinder suspended freely in an ideal fluid with a rigid boundary,

$$F_x = -\frac{\eta\rho_0\pi}{R}(G_1G_2 + L_1L_2 + G_{-1}G_{-2} + L_{-1}L_{-2})$$
$$-\frac{\pi R\rho_0\omega^2}{4c_0^2}\sum_{n=-\infty}^{\infty}(G_nG_{n+1} + L_nL_{n+1} + G_nG_{n-1} + L_nL_{n-1})$$
$$+\frac{\rho_0\pi}{4R}\sum_{n=-\infty}^{\infty}n(n+1)(L_nL_{n+1} + G_nG_{n+1}) + n(n-1)(L_nL_{n-1} + G_nG_{n-1}), \quad (25)$$

$$F_y = \frac{\eta\rho_0\pi}{R}(G_1L_2 - L_1G_2 - G_{-1}L_{-2} + L_{-1}G_{-2})$$
$$-\frac{\pi R\rho_0\omega^2}{4c_0^2}\sum_{n=-\infty}^{\infty}(L_nG_{n+1} - G_nL_{n+1} - L_nG_{n-1} + G_nL_{n-1})$$
$$+\frac{\rho_0\pi}{4R}\sum_{n=-\infty}^{\infty}n(n+1)(L_nG_{n+1} - G_nL_{n+1}) + n(n-1)(G_nL_{n-1} - L_nG_{n-1}). \quad (26)$$

For the long-wavelength approximation ($\alpha R \ll 1$) and $1/(\alpha d)$ has order αR, ARFs on a free cylinder in an ideal fluid with a rigid boundary, i.e., Eqs. (25) and (26) are found to be

$$F_x = \frac{A^2\rho_0\pi}{(\eta+1)R}[(\eta-1)\cos(3\theta) - 2\cos\theta](kR)^3\sin(2kd\cos\theta), \quad (27)$$

$$F_y = \frac{A^2\rho_0\pi}{8(\eta+1)R}\{-(1-\eta)^2[-\sin\theta + \cos(2kd\cos\theta)\sin(3\theta)]$$
$$+4(3-\eta)[\sin\theta + \cos(2kd\cos\theta)\sin\theta]\}(kR)^5. \quad (28)$$

When the plane wave is incident at an angle $\theta = 0$, i.e., the wave propagates along the direction perpendicular to the boundary, Eqs. (27) and (28) can be simplified to

$$F_x = A^2\rho_0\pi\sin(2kd)\frac{(\eta-3)}{(\eta+1)R}(kR)^3, \quad (29)$$

$$F_y = 0. \quad (30)$$

The equations are the same as those in Refs. 26 and 35, except the sign exchanged in the term $(\eta - 3)$, i.e., the positive direction of ARF is altered. The reason is that the positive direction set in our work is different from that in Refs. 26 and 35.

C. Motion of a free cylinder in a viscous fluid under the action of ARFs when a plane wave is incident at an arbitrary angle

Another important work in particle manipulation is the estimation of the trajectory of a free cylinder. The motion of a free cylinder under the action of ARFs [Eqs. (23) and (24)] is described by

$$m\ddot{\mathbf{r}} = \mathbf{F} + \mathbf{F}^{drag} \quad (31)$$

based on the Newton's second law of motion, where $\ddot{\mathbf{r}} = d^2\mathbf{r}/dt^2$ is the acceleration of the cylinder, $m = \pi R^2\rho_1$ is the mass of a unit length of the cylinder, $\mathbf{F}$ is the ARF calculated using formulas (23)

and (24), and $\mathbf{F}^{drag} = -1/2\rho_0\dot{\mathbf{r}}^2 RC_D$ is the viscous drag force of a two-dimensional cylinder,[46,47] with $\dot{\mathbf{r}} = d\mathbf{r}/dt$ being the cylinder velocity, $\mathbf{r} = x\mathbf{e_x} + y\mathbf{e_y}$ the position vector, and C_D the drag coefficient of the cylinder, which has been reported clearly in Ref. 46. In the simulation described in Sec. III F, we use a relation for the drag coefficient as a function of Re, namely, $C_D = (4\pi\zeta/\mathrm{Re})\left[2/\left(1+\sqrt{1+4.3\zeta^2}\right)\right]$ given as Eq. (3.4) in Ref. 46, since Re is small, where $\mathrm{Re} = R\dot{\mathbf{r}}/\nu$ is the Reynolds number while the parameter $\zeta = [0.5 - \gamma - \log(\mathrm{Re}/4)]^{-1}$, with $\gamma = 0.577216$.

Equation (31) can be decomposed into components for the x- and y-directions,

$$m\dot{x}\frac{d\dot{x}}{dx} = F_x + F_x^{drag},$$
$$m\dot{x}\frac{d\dot{y}}{dx} = F_y + F_y^{drag}, \tag{32}$$

by transforming the derivative of time $\ddot{\mathbf{r}} = d^2\mathbf{r}/dt^2$ into the derivative of the coordinate variable x and then the motion trajectory of the particle is obtained combining Runge–Kutta methods.

III. NUMERICAL RESULTS AND DISCUSSIONS

This section performs numerical simulations serially to illustrate the nature and general behavior of the solution. We consider a plane wave with intensity[36] $I_0 = 175.5\ \mathrm{W/m^2}$, which corresponds to a radiator of moderate power, incident upon a rigid cylinder (with a radius $R = 0.1$ mm) at an angle θ ($-\pi/2 \le \theta \le \pi/2$). The cylinder is immersed freely in a viscous fluid (glycerin, density $\rho_0 = 1259.3\ \mathrm{kg/m^3}$, sound speed $c_0 = 1909$ m/s, and kinematic viscosity[44] $\nu = 7.5435 \times 10^{-4}\ \mathrm{m^2/s}$) at a distance d from a rigid boundary. Calculations are performed with a truncation constant of $N_{\max} = M_{\max} = 40$ to ensure convergence to various situations in the simulations.

A. Initial test

A comparison with the result previously presented in Fig. 6(b) of Ref. 27 is performed in Fig. 2 to validate the present formulation. In the figure, the blue dashed line displays the ARF of a fixed cylinder in an ideal fluid for $kR = 0.126$ obtained using Eq. (23) by setting $\eta = 0$, $\lambda' = 0$, $\nu = 0$, and $\mu' = 0$ at an incident angle $\theta = 0$, which means the incident wave is perpendicular to the flat boundary. In this case, $F_y = 0$ and F_x equals the ARF on the fixed cylinder owing to the symmetry of sound field. Parameters I_0, ρ_0, and c_0 are set under the same conditions as Ref. 27. The value of kd in our work ranges from $2kR$ to 6, while $kR < kd < 6$ in Ref. 27. Furthermore, note that the ARF is normalized by $-\rho_0 A^2 R$ since the positive direction set in our work is different from that in Ref. 27. The red markers represent the result exhibited in Fig. 6(b) of Ref. 27. In Fig. 2, an excellent agreement is observed when $2kR < kd < 6$. So the present formulation is effective and valid.

B. Effect of viscosity

Figures 3 and 4 show the ARFs for a free rigid cylinder located a distance $d = 2R$ from the boundary at three selected

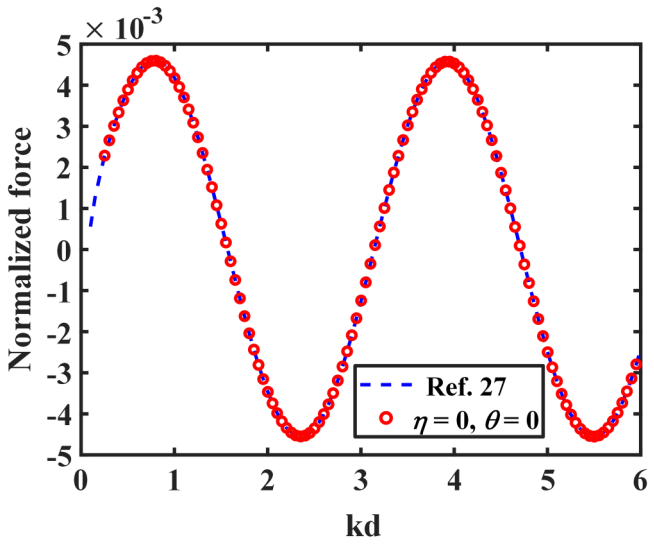

FIG. 2. Normalized ARFs for a fixed rigid cylinder near a rigid boundary in an ideal fluid at $kR = 0.126$ when the incident wave is perpendicular to the boundary.

values of $\delta/R = 0.002$, 0.01, and 0.1 for $\theta = \pi/4$ and $\theta = \pi/2$, respectively. The density ratio $\eta = 1/2$. In Fig. 3(a), the amplitude of F_x decreases for a small particle with increasing δ/R (i.e., increasing viscosity). For a large particle, F_x starts to increase with increasing δ/R. This behavior is not the same for F_y in Fig. 3(b), which always decreases with increasing viscosity. This means the amplitude of the total ARF may decrease at certain values of kR for increasing viscosity in the case that $\theta = \pi/4$. This phenomenon is significantly different from the case of a rigid cylinder immersed in a boundless viscous fluid domain.[44] In Figs. 4(a) and 4(b), we consider the special case that $\theta = \pi/2$, where the incident wave is parallel to the boundary. The amplitude of F_x always increases with increasing viscosity. However, for F_y, the amplitude always decreases with increasing viscosity. Moreover, the amplitude of F_x is very smaller than that of F_y and tends to zero when the viscosity is low. A comparison of Figs. 3 and 4 shows that the viscous effects for the case of a cylinder in a bounded viscous fluid domain are smaller than those in a boundless viscous fluid domain, especially for a small particle. F_x behavior depends on kR, while F_y always decreases with increasing viscosity under these conditions. The reason is that F_y is positive, i.e., the particle is attracted to the velocity antinode, the largest contribution to the ARF is the velocity contribution. As the viscosity increases, the decrease in the velocity is more than that in the pressure. Therefore, the amplitude of F_y decreases with increasing viscosity.[48]

C. Effects of the incident angle of incident wave and the position of the cylinder

Figure 5 presents ARFs for a rigid cylinder free to move in a viscous fluid (glycerin) vs the incident angle θ and dimensionless distance d/R at $kR = 0.5$. The dimensionless distance varies

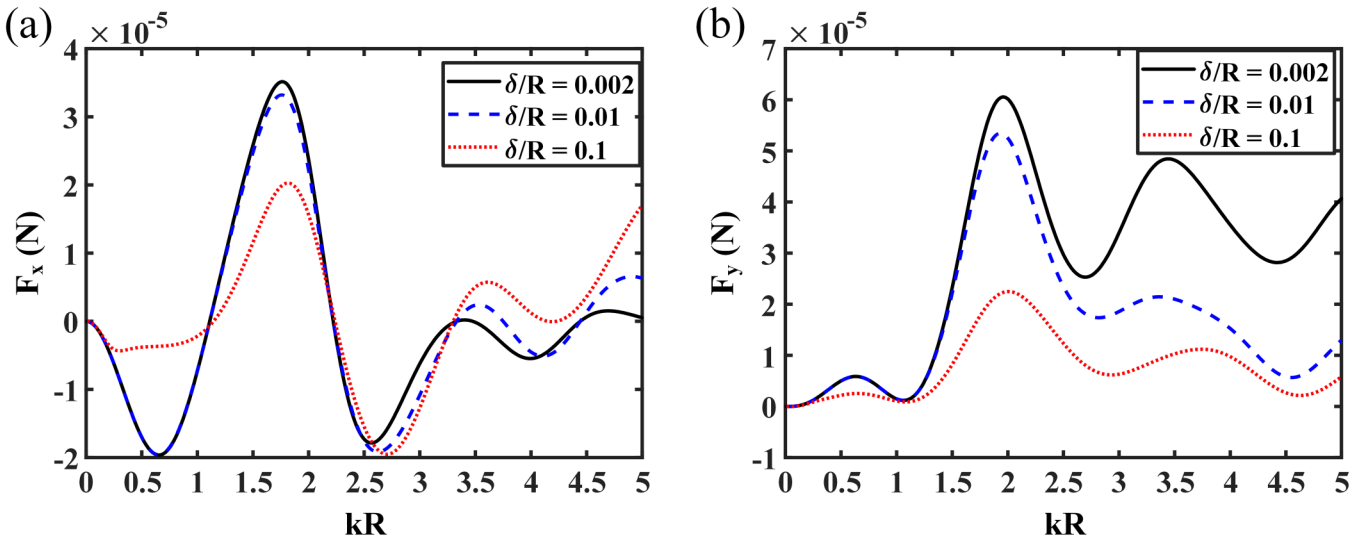

FIG. 3. ARFs for a free cylinder in a viscous fluid with a rigid boundary at different δ/R when $\theta = \pi/4$. (a) F_x defined in Eq. (23) and (b) F_y defined in Eq. (24).

between 2 and 10. The incident angle θ ranges from $-\pi/2$ to $\pi/2$ scanning the whole sound field. The density ratio $\eta = 1/2$. The axial ARFs are presented in Fig. 5(a). It is noted that $F_x(\theta) = F_x(-\theta)$ with respect to the axis $\theta = 0$ as increasing θ. At $\theta = 0$, the reflected wave from the boundary becomes strong and the amplitude of F_x is maximum. However, the maximum F_x is positive or negative depending on the choice of d/R, i.e., the particle is repelled away from or pulled toward the sound source for a certain d/R. Figure 5(b) exhibits the transverse ARFs, which shows that $F_y(\theta) = -F_y(-\theta)$ with respect to the axis $\theta = 0$. F_y vanishes at $\theta = 0$ owing to symmetry of sound field and occurs maximum amplitude at $|\theta| = \pi/2$.

Figure 6 displays the ARFs for a rigid cylinder immersed freely in a viscous fluid (glycerin) vs the dimensionless parameter kR and d/R at $\theta = \pi/4$. The density ratio $\eta = 1/2$. Figures 6(a) and 6(b) show that the peaks and dips of F_x and F_y vs kR become more densely packed as d/R increases. This phenomenon is mainly caused by the interaction of the fields scattered and reflected by the

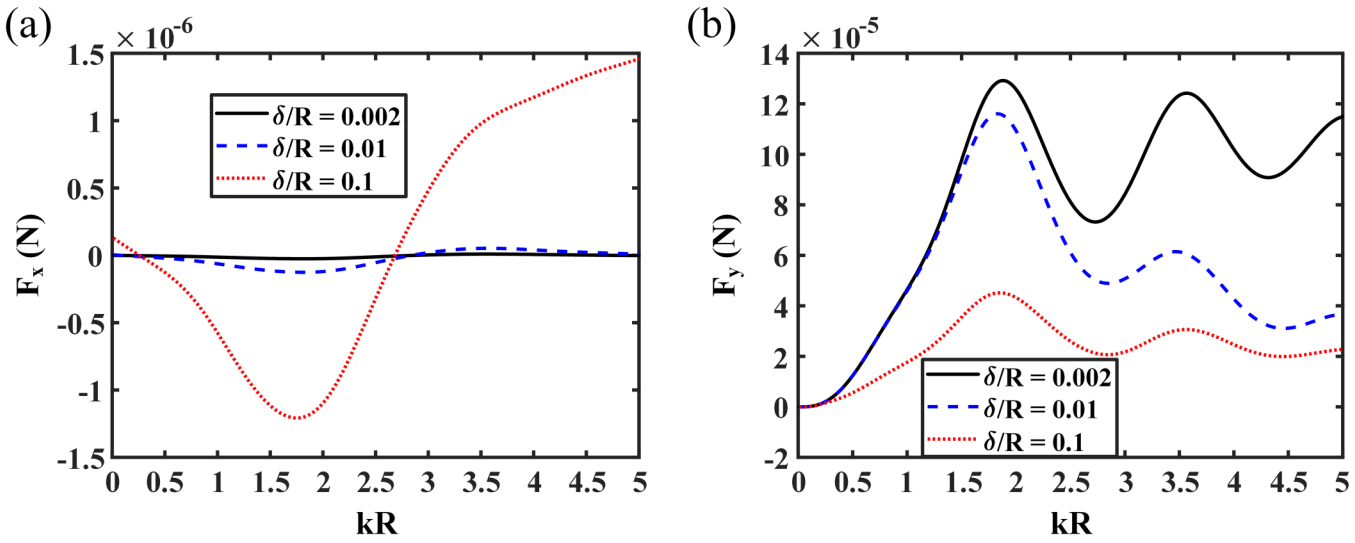

FIG. 4. ARFs for a free cylinder in a viscous fluid with a rigid boundary at different δ/R when $\theta = \pi/2$. (a) F_x defined in Eq. (23) and (b) F_y defined in Eq. (24).

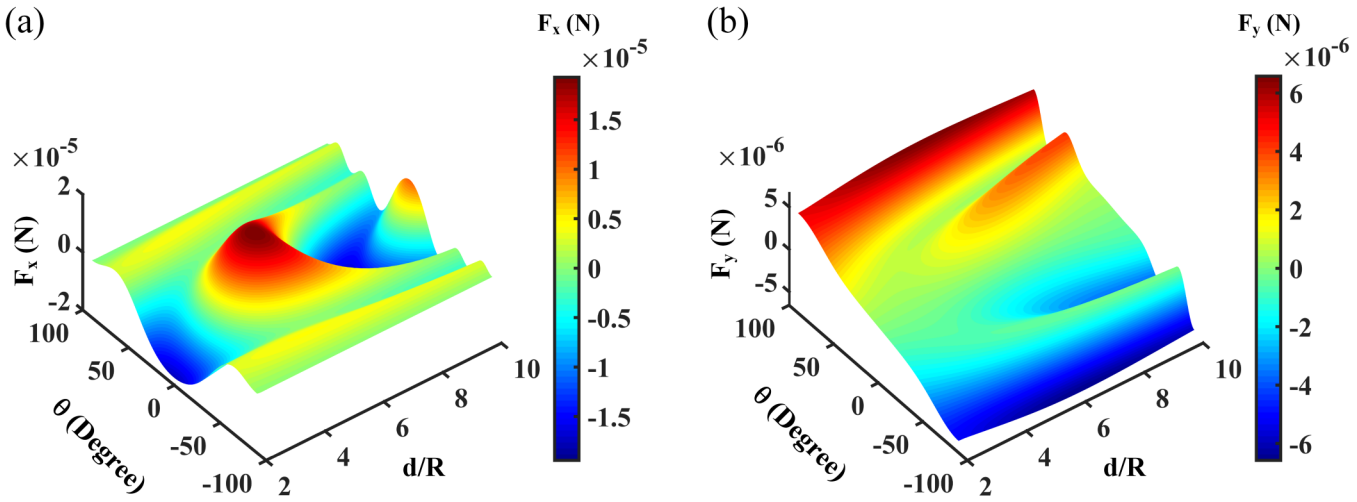

FIG. 5. ARFs for a free cylinder in a viscous fluid vs θ and d/R at $kR = 0.5$ and $\eta = 1/2$. (a) F_x defined in Eq. (23) and (b) F_y defined in Eq. (24).

particle and boundary. Or, specifically speaking, it is owing to the phase difference between the real and image cylinders oscillates increasingly faster as d/R grows.[49,50] In addition, d/R does not have a prominent effect on the ARFs for small kR. This may be explained by the fact that the wavelength is so long compared with the particle size that the particle is almost nonexistent for the incident wave. ARFs for large kR vary periodically with d/R. Moreover, ARFs are positive and negative depending on the choice of kR and d/R for a selected θ, indicating that the particle may be captured under certain conditions. Note that the particle is attracted to the velocity antinode when the ARF is positive and to the pressure antinode when the ARF is negative. A stable equilibrium of the particle is achieved when the slope of the ARF to d/R is negative.[51,52] In this case, the particle can be stably manipulated. Therefore, we can choose effective parameters to achieve more accurate and effective particle control.

D. Effect of the density ratio η

Figure 7 exhibits the effect of η on the ARFs for a freely moving rigid cylinder. Parameters are set as $\delta/R = 0.1$, $\theta = \pi/4$, $0 \le \eta \le 6$, and $2 \le d/R \le 6$. Figure 7 reveals that η has a considerable effect on the magnitudes and directions of F_x and F_y, and it can be a significant fraction of ARF. F_x and F_y decrease and then

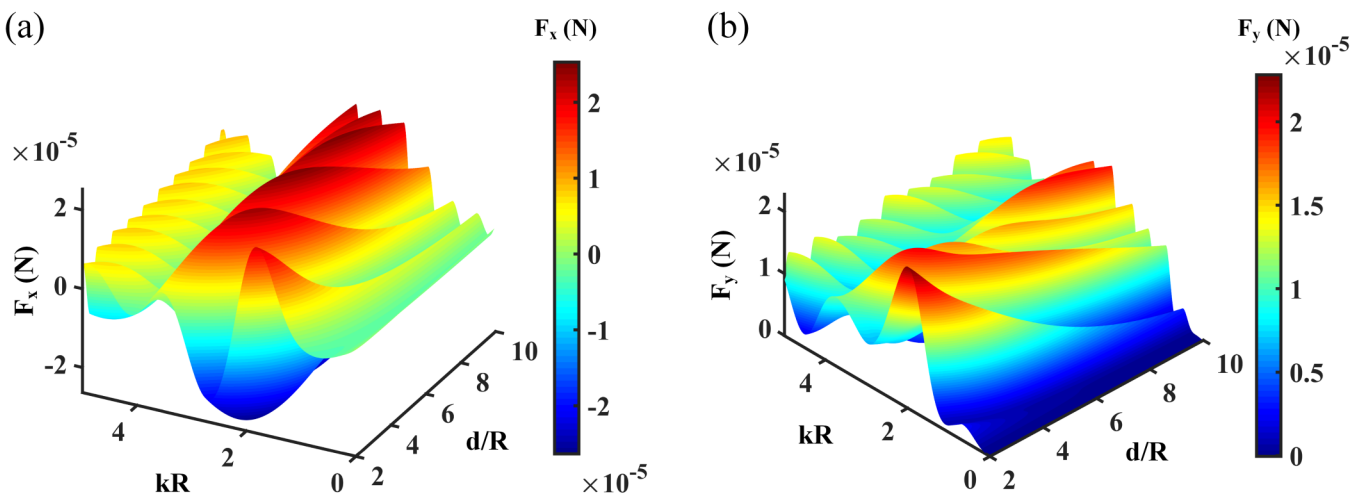

FIG. 6. ARFs for a rigid cylinder immersed freely in a viscous fluid vs kR and d/R at $\theta = \pi/4$ and $\eta = 1/2$. (a) F_x defined in Eq. (23) and (b) F_y defined in Eq. (24).

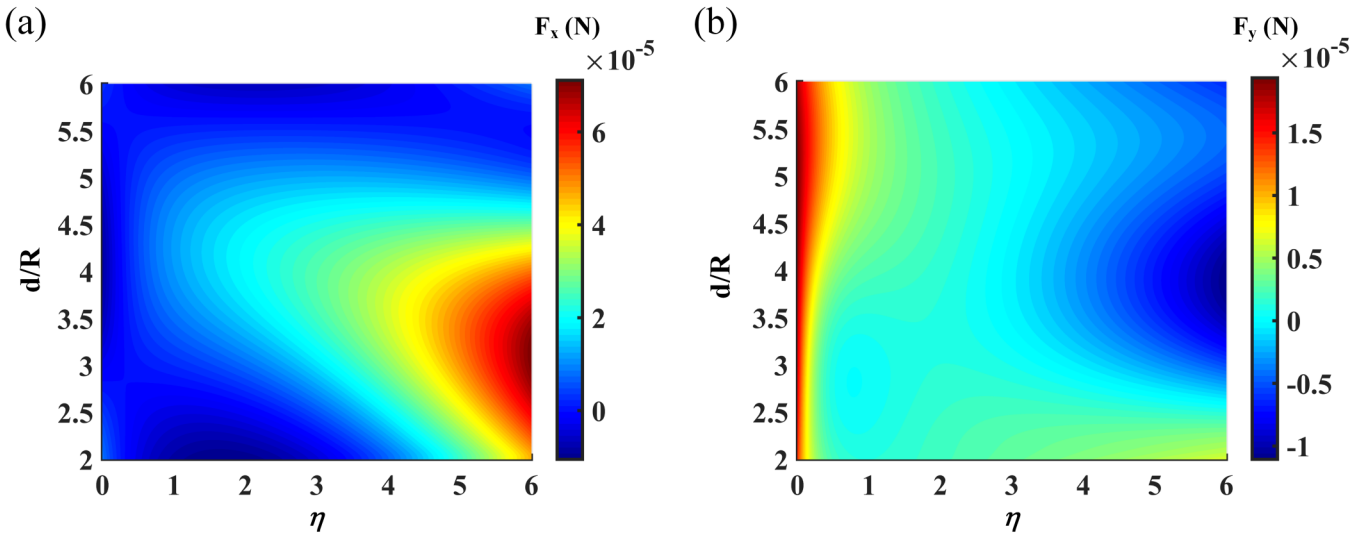

FIG. 7. ARFs for a free cylinder in a viscous fluid vs η and d/R at $\delta/R = 0.1$ and $\theta = \pi/4$. (a) F_x defined in Eq. (23) and (b) F_y defined in Eq. (24).

increase after a critical value with increasing η while the particle is close to the boundary (small d/R). At large d/R, F_x increases, whereas F_y decreases as η increases.

E. Comparison of ARFs in four cases: free cylinder, fixed cylinder, viscous liquid, and ideal liquid

Figures 8 compares the ARFs in the four cases of free cylinder, fixed cylinder, viscous liquid, and ideal liquid to examine the behavior of ARFs under these conditions. Factors affecting the ARF

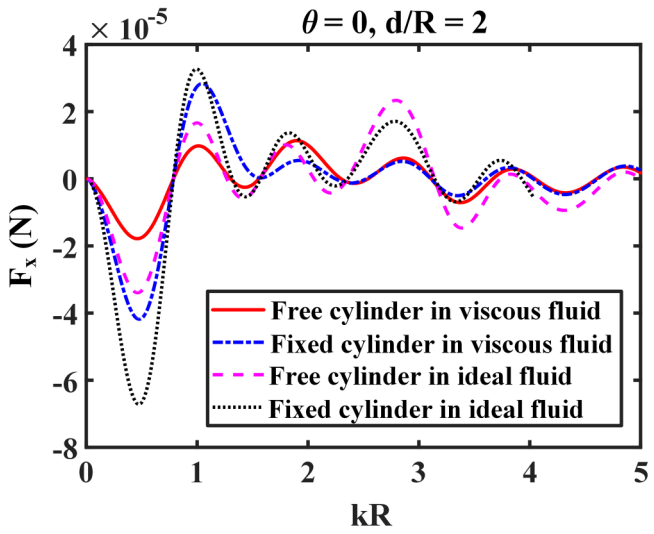

FIG. 8. ARFs in four cases: a free cylinder, a fixed cylinder, viscous liquid, and ideal liquid.

are various. Here, a special incidence angle $\theta = 0$, where the incident wave is perpendicular to the boundary, is considered as the best help to reveal the physics of the problem. In this case, F_x is the resultant force and $F_y = 0$ owing to the symmetry of sound field. Parameters are set as $\eta = 1/2$ and $d/R = 2$. The curves in Fig. 8 show that the ARF on the fixed cylinder is much more than that on the free cylinder immersed in the same fluid for small kR. A similar conclusion for a rigid sphere was described in Ref. 37. With increasing kR, the difference of ARFs between the free particle and fixed particle decreases in the same fluid and even tends to zero in a viscous liquid. For particles in the same state, the ARF in a viscous liquid is smaller than that in an ideal liquid for the current conditions. The reason is that the acoustic pressure decreases due to the effect of viscosity in this case. Consequently, the ARF owing to the acoustic pressure decreases compared with that in an ideal fluid.

Figures 9(a)–9(c) show the axial ARFs on a rigid cylinder immersed freely in an ideal fluid computed by the two methods of the exact theory [Eq. (25)] and approximate formulas [Eq. (29)]. The parameters are the same as those for Fig. 8, except that $kR = 0.005$, 0.01, and 0.015 and kd ranges from $2kR$ to $6kR$. Moreover, the relative percentage errors of the ARFs obtained by these two methods for different kR are presented in Fig. 9(d). It seen that the ARFs are negative and the cylinder moves to the boundary. The errors of the approximate results are less than 5.3% for all cases mentioned. Errors become more and more significant with the increase of kR and the decrease of kd. But For small kR and large kd, the approximate results can achieve a good agreement with the exact solutions.

F. Motion of a freely moving rigid cylinder

We next calculate the trajectories of the cylinder under different conditions using Eqs. (31) and (32). Results are shown in Fig. 10. Circles and arrows mark the initial and final positions of

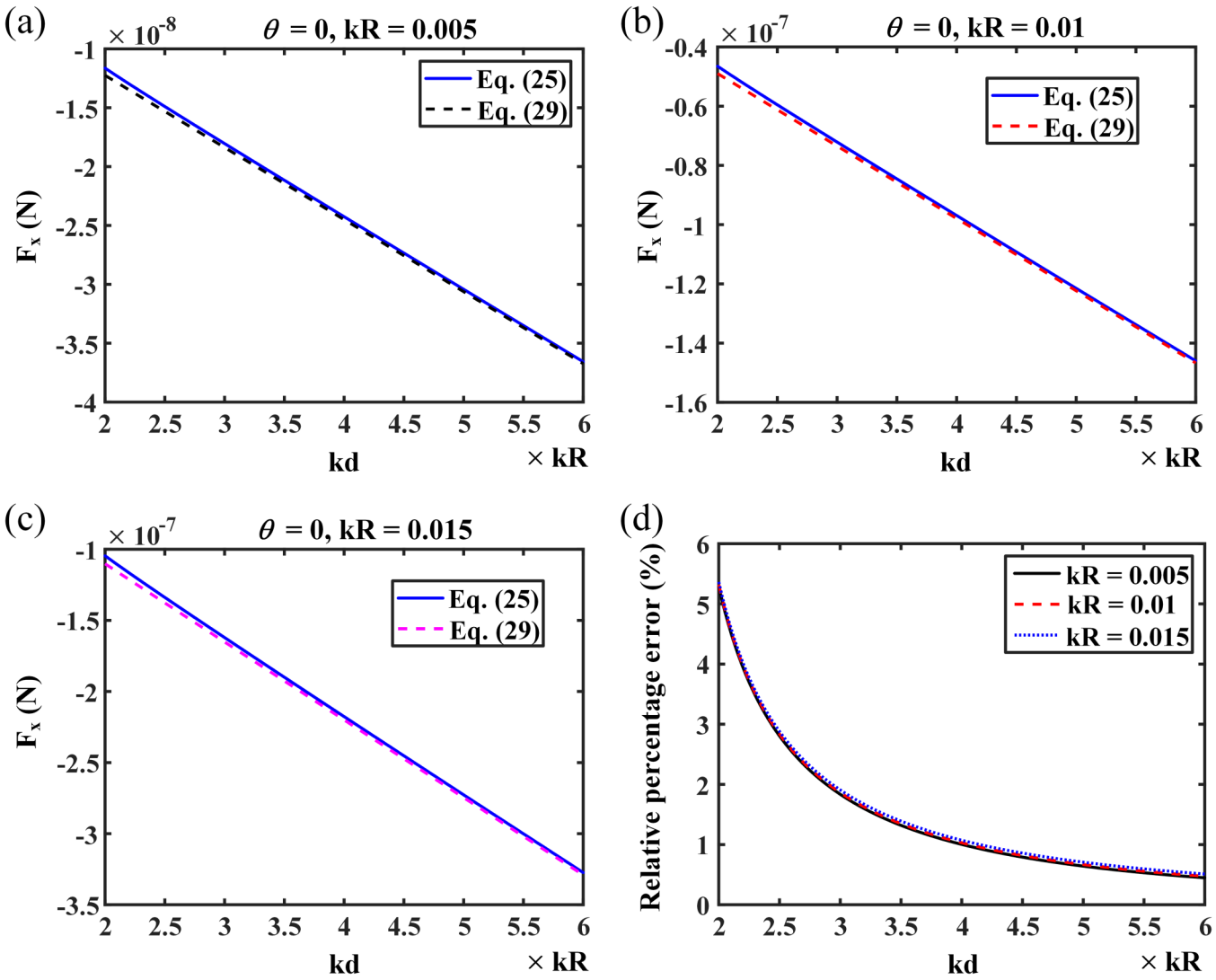

FIG. 9. Comparisons of the ARFs obtained adopting two methods of the exact theory and approximate formulas at different kR for $\theta = 0$ and $\eta = 1/2$. (a)–(c) The ARFs for $kR =$ 0.005, 0.01, and 0.015, respectively. (d) The relative percentage errors.

particles, respectively. Figure 10(a) presents the trajectories of the rigid cylinder with radius $R = 0.1$ mm and $R = 0.2$ mm for varied incident angles, where $-x = d$ ranges from 2 to 11, $\eta = 0.1$, and $kR = 0.5$. In Fig. 10(a), the black line and red line correspond to $R = 0.1$ mm and $R = 0.2$ mm, respectively. The solid line, dashed-dotted line, and dashed line correspond to $\theta = 0$, $\theta = \pi/4$, and $\theta = -\pi/2$, respectively. At the initial position, particles have an initial velocity $v_0 = \dot{r}_0 = 10^{-5}$ m/s along the x axis. Figure 10(a) shows that the trajectories of particles change with θ. Taking the particle with radius $R = 0.1$ mm as an example, the particle initially moves along the negative x axis. Then, the particle keeps moving under the acceleration along the negative x axis and positive y axis and turns to the negative y direction after θ is converted into $-\pi/2$ from $\pi/4$. The particle can thus be regulated by adjusting the incident angle. Furthermore, observing particle trajectories with various radii, we find that trajectories are different under external conditions that are strictly the same. This means that particle separation and screening can be achieved by manipulating particles with ARF. In Figs. 10(b)–10(e), we consider other factors affecting the motion trajectories, such as δ/R, η, kR, and the initial velocity. A comparison with the case represented by solid lines in Figs. 10(b)–10(e) ($R = 0.1$ mm $\theta = \pi/4$, $\delta/R = 0.1$, $\eta = 0.5$, $kR = 0.5$, $v_0 = 10^{-5}$ m/s) reveals that trajectories change if one of the parameters alters. Therefore, as long as the particle size and external conditions are known, we can predict and regulate the particle trajectory under the effect of ARF, allowing not only the

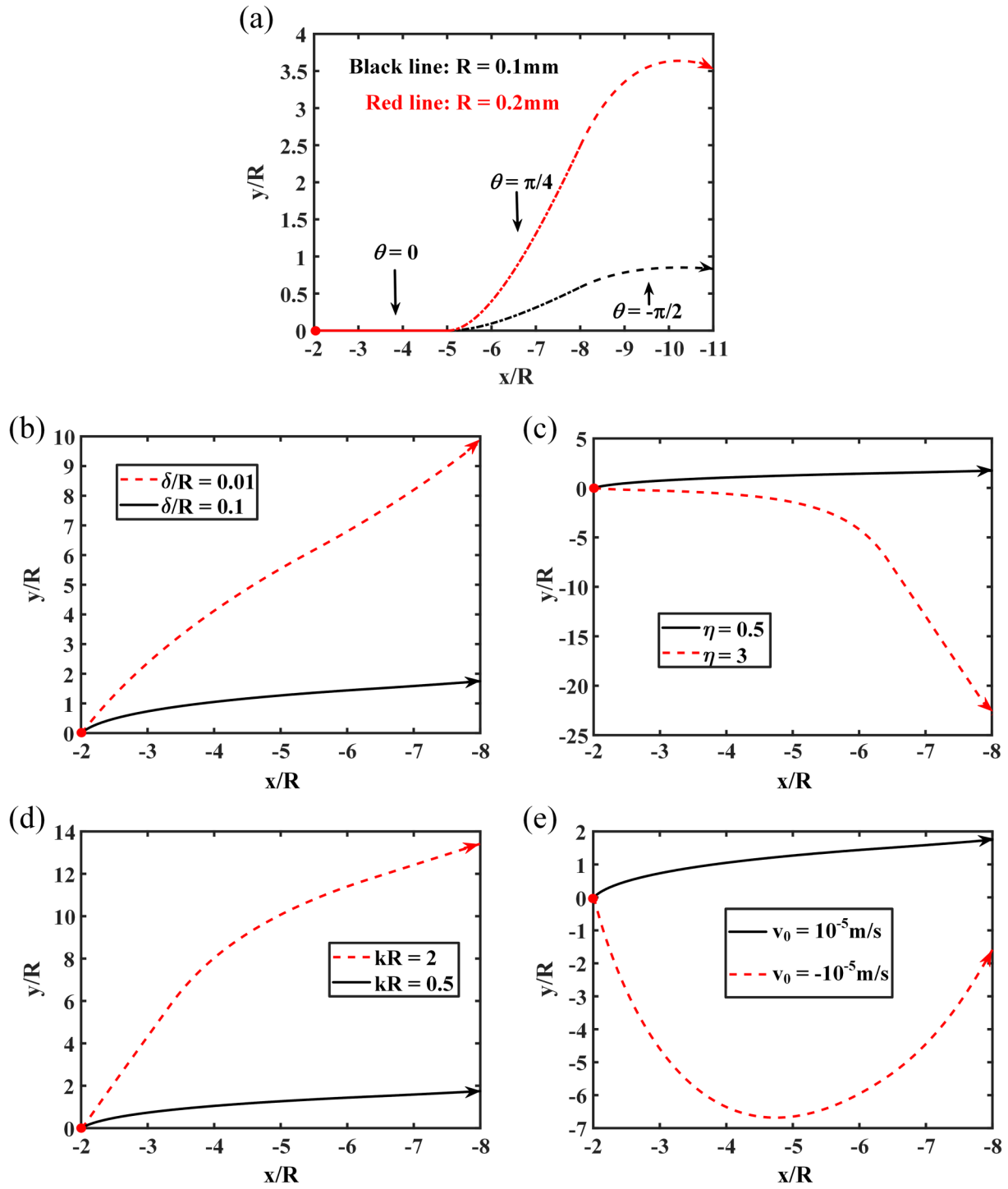

FIG. 10. Motion trajectories of a rigid cylinder under different conditions. (a) Motion trajectories of the rigid cylinder with radius $R = 0.1$ mm and $R = 0.2$ mm for varied incident angles, respectively. Solid lines, dashed-dotted lines, and dashed line correspond to $\theta = 0$, $\theta = \pi/4$, and $\theta = -\pi/2$, respectively. (b) Motion trajectories of the rigid cylinder with radius $R = 0.1$ mm for different δ/R. (c) Motion trajectories of the rigid cylinder with radius $R = 0.1$ mm for different η. (d) Motion trajectories of the rigid cylinder with radius $R = 0.1$ mm for different kR. (e) Motion trajectories of the rigid cylinder with radius $R = 0.1$ mm for different initial velocities.

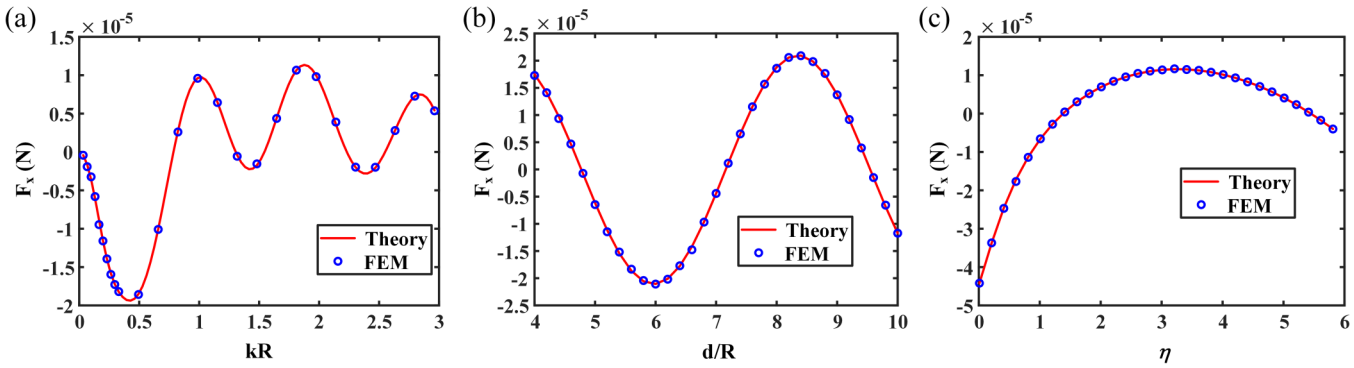

FIG. 11. Comparisons of the theory and FEM for different cases with $\theta = 0$. (a) ARFs vs kR for $\eta = 0.5$ and $d/R = 2$. (b) ARFs vs d/R for $\eta = 0.5$ and $kR = 0.658$ (c) ARFs vs η for $kR = 0.658$ and $d/R = 6$.

capture of particles individually but also their assembly to form clusters of precisely assembled objects in future applications.

IV. FINITE ELEMENT SIMULATIONS

To further verify the theoretical solutions, we perform numerical simulations using a finite element solver (COMSOL Multiphysics FEM software) in this section. The lower boundary of the computational domain is set as a no-slip hard boundary. Absorbing boundary conditions delimit the computational domain to simulate the semi-infinite field. The surface of the cylinder is set as a rigid boundary. A boundary layer is added around the particle to analyze the penetration depth of the viscous wave. For comparison, parameters are selected as in the theoretical calculations in subsequent simulations. ARFs are evaluated using Eq. (21).

Figures 11(a)–11(c) show the ARFs computed adopting theory and the FEM for different cases with $\theta = 0$. Figure 11(a) plots the ARFs vs kR for $\eta = 0.5$ and $d/R = 2$. Results of the ARFs vs d/R for $\eta = 0.5$ and $kR = 0.658$ are presented in Fig. 11(b). The effect of η at $kR = 0.658$ and $d/R = 6$is considered in Fig. 11(c). Figure 12 presents axial and transverse ARFs for various θ at $d/R = 6$, $kR = 0.658$, and $\eta = 0.5$. It is obvious that results obtained adopting the FEM and those calculated theoretically are in good agreement. These comparisons illustrate that our present formulations are feasible for the assumptions made.

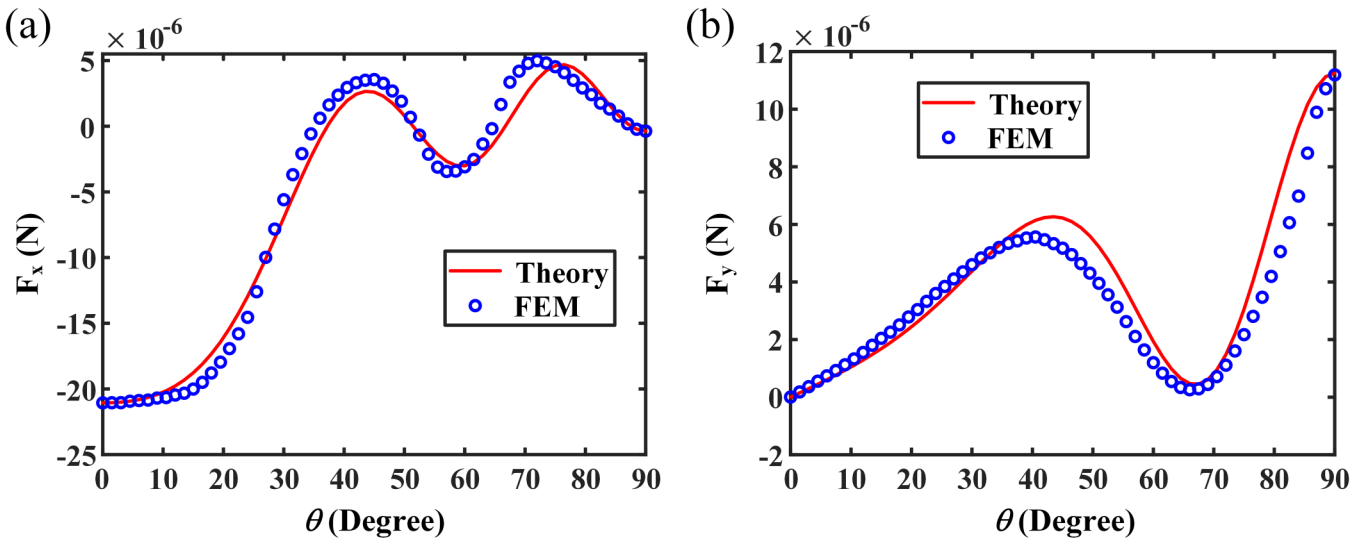

FIG. 12. Comparisons of the theory and FEM for various θ at selected $d/R = 6$, $kR = 0.658$, and $\eta = 0.5$. (a) F_x vs θ. (b) F_y vs θ.

V. CONCLUSIONS

The present paper gave an analytical solution computational description, graphic illustration, and physical explanation of the title problem. An approximate expression of ARFs was proposed in the case of a long-wavelength approximation. Numerical results showed that the magnitude and direction of ARF on a rigid cylinder freely in a viscous fluid with a boundary depend on various factors, such as fluid viscosity, incident angle of the plane wave, density ratio of the fluid to particle, particle radius, and position. In addition, the amplitude of the total ARF on a freely moving rigid cylinder illuminated by an incident wave at a certain angle maybe decrease with increasing viscosity, which is significantly different from the case of a rigid cylinder immersed in a boundless viscous fluid domain. Additionally, the ARF on the fixed cylinder is much larger than that on the free cylinder for small kR but the difference of them decreases with increasing kR. Furthermore, the trajectory of the particle changes if one of the parameters affecting ARFs alters. We can therefore predict and regulate particle trajectories by selecting appropriate parameters, allowing not only the capture of particles individually but also their assembly to form clusters of precisely assembled objects in future applications. Finally, we compared the results of theory and FEM for different cases. The FEM results and theoretical results are in a good agreement, substantiating our theoretical predictions. This work helps better understand the underlying mechanism of particle manipulation using ARF and will undoubtedly increase the design quality of acoustic manipulation devices. The results can readily be extended to related situations, such as those involving free cylinders with different mechanical properties and multilayer cylinder.

ACKNOWLEDGMENTS

This work was supported by National Key R & D Program of China (No. 2017YFA0303702), State Key Program of National Natural Science of China (No. 11834008), National Natural Science Foundation of China (NNSFC) (No. 11774167), State Key Laboratory of Acoustics, Chinese Academy of Science (No. SKLA202008), Key Laboratory of Underwater Acoustic Environment, Chinese Academy of Sciences (No. SSHJ-KFKT-1701), and AQSIQ Technology R&D Program, China (No. 2017QK125).

DATA AVAILABILITY

The data that support the findings of this study are available from the corresponding author upon reasonable request.

REFERENCES

[1]M. K. Nichols, R. K. Kumar, P. G. Bassindale, L. Tian, A. C. Barnes, B. W. Drinkwater, A. J. Patil, and S. Mann, Small **14**, 1800739 (2018).
[2]M. Saito, T. Daian, K. Hayashi, and S. Izumida, J. Appl. Phys. **83**, 3490 (1998).
[3]L. Tian, N. Martin, P. G. Bassindale, A. J. Patil, M. Li, A. Barnes, B. W. Drinkwater, and S. Mann, Nat. Commun. **7**, 13068 (2016).
[4]L. Meng, F. Cai, F. Li, W. Zhou, L. Niu, and H. Zheng, J. Phys. D Appl. Phys. **52**, 273001 (2019).
[5]J. R. Wu, J. Acoust. Soc. **89**, 2140 (1991).
[6]A. Ozcelik, J. Rufo, F. Guo, Y. Gu, P. Li, J. Lata, and T. J. Huang, Nat. Methods **15**, 1021 (2018).
[7]A. Sarvazyan and S. Tsyuryupa, Proc. Mtgs. Acoust. **26**, 020002 (2016).
[8]J. Shi, D. Ahmed, X. Mao, S. C. Lin, A. Lawit, and T. J. Huang, Lab Chip **9**, 2890 (2009).
[9]J. Lee, S. Y. Teh, A. Lee, H. H. Kim, C. Y. Lee, and K. K. Shung, Appl. Phys. Lett. **95**, 073701 (2009).
[10]N. L. Shirokova, in *Physical Principles of Ultrasonic Technology*, edited by L. D. Rosenberg (Plenum, New York, 1973), Vol. 2, pp. 475–539.
[11]M. X. Wu *et al.*, Small **14**, 1801131 (2018).
[12]A. P. Sarvazyan, O. V. Rudenko, and W. L. Nyborg, Ultrasound Med. Biol. **36**, 1379 (2010).
[13]L. V. King, Phys. R. Soc. Lond. A Mat. **147**, 212 (1934).
[14]K. Yosioka and Y. Kawasima, Acustica **5**, 167 (1955).
[15]J. Awatani, J. Acoust. Soc. Jpn. **9**, 140 (1953).
[16]J. R. Wu and G. H. Du, J. Acoust. Soc. Am. **87**, 997 (1990).
[17]T. Hasegawa, K. Saka, N. Inoue, and K. Matsuzawa, J. Acoust. Soc. Am. **83**, 1770 (1988).
[18]R. R. Wu, K. X. Cheng, X. Z. Liu, J. H. Liu, Y. W. Mao, and X. F. Gong, J. Appl. Phys. **116**, 144903 (2014).
[19]Y. P. Qiao, X. F. Zhang, and G. B. Zhang, J. Acoust. Soc. Am. **141**, 4633 (2017).
[20]X. F. Zhang, Z. G. Song, D. M. Chen, G. B. Zhang, and H. Cao, J. Acoust. Soc. Am. **137**, 1826 (2015).
[21]C. Jiang, X. Z. Liu, J. H. Liu, Y. W. Mao, and P. L. Marston, Ultrasonics **76**, 1 (2017).
[22]P. L. Marston, J. Acoust. Soc. Am. **120**, 3518 (2006).
[23]J. Y. Shi, X. F. Zhang, R. M. Chen, and G. B. Zhang, Wave Motion **80**, 37 (2018).
[24]A. K. Miri and F. G. Mitri, Ultrasound Med. Biol. **37**, 301 (2011).
[25]H. B. Wang, S. Gao, Y. P. Qiao, J. H. Liu, and X. Z. Liu, Phys. Fluids **31**, 047103 (2019).
[26]W. Wei, D. B. Thiessen, and P. L. Marston, J. Acoust. Soc. Am. **116**, 201 (2004).
[27]J. Wang and J. Dual, Ultrasonics **52**, 325 (2012).
[28]T. F. W. Embleton, J. Acoust. Soc. Am. **26**, 40 (1954).
[29]G. T. Silva, J. Acoust. Soc. Am. **130**, 3541 (2011).
[30]D. Baresch, J. L. Thomas, and R. Marchiano, J. Acoust. Soc. Am. **133**, 25 (2013).
[31]J. P. Leão-Neto and G. T. Silva, Ultrasonics **71**, 1 (2016).
[32]J. P. Leão-Neto, J. H. Lopes, and G. T. Silva, Phys. Rev. Appl. **6**, 024025 (2016).
[33]P. J. Westervelt, J. Acoust. Soc. Am. **23**, 312 (1951).
[34]A. N. Guz and A. P. Zhuk, Dokl. Akad. Nauk SSSR **266**, 32 (1982).
[35]A. N. Guz, A. P. Zhuk, and P. L. Marston, J. Fluids Struct. **25**, 1206 (2009).
[36]A. N. Guz and A. P. Zhuk, Int. Appl. Mech. **40**, 246 (2004).
[37]A. A. Doinikov, Proc. R. Soc. Lond. A **447**, 447 (1994).
[38]S. D. Danilov and M. A. Mironov, Sov. Phys. Acoust. **30**, 276 (1984).
[39]S. D. Danilov and M. A. Mironov, J. Acoust. Soc. Am. **107**, 143 (2000).
[40]J. Wang and J. Dual, J. Acoust. Soc. Am. **129**, 3490 (2011).
[41]S. Sepehrirahnama, F. S. Chau, and K. M. Lim, Phy. Rev. E **93**, 023307 (2016).
[42]S. Sepehrirahnama, F. S. Chau, and K. M. Lim, Phy. Rev. E **92**, 063309 (2015).
[43]N. Guz, Dokl. Akad. Nauk SSSR **253**, 825 (1980).
[44]W. H. Lin and A. C. Raptis, J. Acoust. Soc. Am. **73**, 736 (1983).
[45]D. E. Gray, in *American Institute of Physics Handbook*, 3rd ed. (McGraw-Hill, New York, 1972).
[46]A. Khalili and B. Liu, J. Fluid Mech. **817**, 374 (2017).
[47]F. M. White, *Fluid Mechanics*, 8rd ed. (McGraw-Hill, New York, 2015).
[48]D. Foresti, M. Nabavi, and D. Poulikakos, J. Fluid Mech. **709**, 581 (2012).
[49]S. M. Hasheminejad and S. A. Badsar, Q. J. Mech. Appl. Math. **57**, 95 (2004).
[50]S. M. Hasheminejad and M. A. Alibakhshi, Int. J. Mech. Sci. **49**, 1 (2007).
[51]S. Xu, C. Qiu, and Z. Liu, Europhys. Lett. **99**, 44003 (2012).
[52]F. P. Beer, E. R. Johnston, D. F. Mazurek, P. J. Cornell, and E. R. Eisenberg, *Vector Mechanics for Engineers Statics and Dynamics*, 9th ed. (McGraw-Hill, New York, 2009), p. 158.